

OMEGAS: Object Mesh Extraction from Large Scenes Guided by Gaussian Segmentation

Lizhi Wang*, Feng Zhou*, Bo Yu, Pu Cao, Jianqin Yin†,

Beijing University of Posts and Telecommunications
Beijing, China
wanglizhi@bupt.edu.cn

Abstract

Recent advancements in 3D reconstruction technologies have paved the way for high-quality and real-time rendering of complex 3D scenes. Despite these achievements, a notable challenge persists: it is difficult to precisely reconstruct specific objects from large scenes. Current scene reconstruction techniques frequently result in the loss of object detail textures and are unable to reconstruct object portions that are occluded or unseen in views. To address this challenge, we delve into the meticulous 3D reconstruction of specific objects within large scenes and propose a framework termed **OMEGAS: Object Mesh Extraction from Large Scenes Guided by GAussian Segmentation**. Specifically, we proposed a novel 3D target segmentation technique based on 2D Gaussian Splatting, which segments 3D consistent target masks in multi-view scene images and generates a preliminary target model. Moreover, to reconstruct the unseen portions of the target, we propose a novel target replenishment technique driven by large-scale generative diffusion priors. We demonstrate that our method can accurately reconstruct specific targets from large scenes, both quantitatively and qualitatively. Our experiments show that OMEGAS significantly outperforms existing reconstruction methods across various scenarios.

Introduction

In recent years, the field of 3D reconstruction has emerged as a pivotal area of research, driven by its profound applications across a diverse range of disciplines, including robotics (Siciliano, Khatib, and Kröger 2008), architectural design (Caetano, Santos, and Leitão 2020), virtual reality (Xiong et al. 2021), and so on. The community has successfully achieved high-quality, real-time reconstruction and rendering of complex 3D scenes, largely due to the advancement of 3D rendering-based models (Mildenhall et al. 2020; Barron et al. 2022; Yu et al. 2021; Kerbl et al. 2023; Wu et al. 2023; Yang et al. 2023).

However, existing methods struggle to reconstruct a specific target object’s 3D mesh in high-quality given scene images, which is somehow more solid and straightforward in downstream applications like virtual game modeling. This

*These authors contributed equally.

†Corresponding author

Copyright © 2025, Association for the Advancement of Artificial Intelligence (www.aaai.org). All rights reserved.

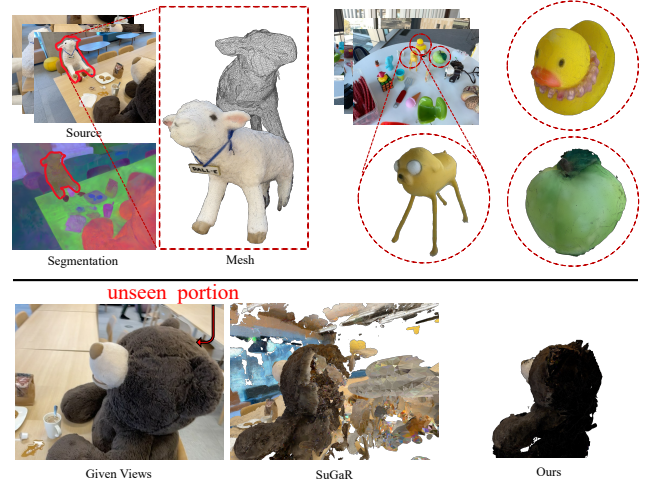


Figure 1: OMEGAS segments and generates high-quality meshes for specified objects in open-world scenes (top). OMEGAS can effectively reconstruct the unseen portion of the target (bottom).

challenge is particularly evident in two key aspects. First, the reconstruction of entire scenes often leads to a compromise in the quality of specific object reconstruction. Besides, certain parts of a specific object in a scene are frequently occluded or invisible from any perspective, making their reconstruction challenging with current methods, as illustrated in Figure 1 bottom.

In this paper, we propose a novel and effective framework that reconstructs the 3D mesh of the target object given multi-view open-world scene images, termed OMEGAS: Object Mesh Extraction from Large Scenes Guided by GAussian Segmentation. As shown in Figure 1 top, given the multi-view scene images, our framework can freely select and segment the target object from images and extract the complete 3D object mesh.

Specifically, we propose a novel 3D target segmentation technique based on 2D Gaussian Splatting (2DGS) (Huang et al. 2024). Inspired by Gaussian Grouping (Ye et al. 2023), we first utilize the SAM (Kirillov et al. 2023) to provide initial target segmentation masks in multi-view scenes. Then,

we input the masks along with the scene images into a 2DGS model and introduce a unique compact identity vector as a supervisory signal, enabling 3D segmentation within the 2DGS space. By leveraging the 3D consistency of the 2DGS model, we can iteratively optimize the segmentation results of the target within the scene, ultimately obtaining precise 2D segmentation results along with an initial 3D model of the target.

Subsequently, to address the occluded portions of the target that cannot be directly reconstructed, we leverage large-scale, open-world generative priors such as Stable Diffusion (Rombach et al. 2022). Specifically, we segment the target from the original perspective and then use these target-only images to personalize Stable Diffusion. This approach allows for the concentration of knowledge on the specific target. Our goal is to utilize the customized Stable Diffusion to assist inpainting the incomplete faces of the target Gaussian model. In this process, we propose a novel mask generation technique based on the diffusion denoising process to mark the under-constructed portions of the novel-view rendered images. Ultimately, we further train the 2DGS model with additional inpainted view images to obtain the final, fully completed target mesh.

Extensive experiments demonstrate the superior performance of our framework, capable of reconstructing the target object mesh with high precision.

In summary, our contributions are:

- We propose OMEGAS, an effective framework to extract meshes of specified objects through multi-view 2D images in open-world scenes.
- We propose a novel 3D target segmentation technique based on 2D Gaussian Splatting to extract the target 3D model from multi-view scene images and create 3D-consistent target masks. Furthermore, we introduce a novel target replenishment technique by leveraging large-scale generative diffusion priors to adaptively optimize the unseen portions of the target.
- Extensive experiments reveal that OMEGAS operates effectively in a range of open-world scenes and significantly surpasses the existing approach in performance. Specifically, our approach shows superiority in both texture details and occlusion robustness on target object reconstruction.

Related Works

Segmentation of Rendering-based 3D Models

Due to the intrinsic implicit nature of the rendering-based model, it’s hard to do normal data-driven training for semantic segmentation like explicit 3D models (*e.g.*, 3D point-cloud segmentation (Xu et al. 2020; Fan et al. 2021)). To address this issue, Spin-NeRF (Fan et al. 2021) first proposes a method that segments specific objects in NeRF and achieves inpainting in different views with 3D consistency. Recently, 3D Gaussian Splatting established its effectiveness in the reconstruction task exhibiting high inference speeds and remarkable quality. Following Spin-NeRF, Gaussian Grouping (Ye et al. 2023) extends the object-oriented concept from

Spin-NeRF to 3D Gaussian Splatting, enabling the joint reconstruction and segmentation of anything in open-world 3D scenes and various 3D editing tasks.

Mesh Extraction from Images

In the early days, the development of Structure-from-motion (SfM) (Snavely, Seitz, and Szeliski 2006) and Multi-View Stereo (MVS) (Goesele et al. 2007) allows for 3D reconstruction from multi-view images. More recently, owing to the development of neural network-based 3D reconstruction method (Mildenhall et al. 2020; Kerbl et al. 2023), various approaches have explored integrating rendering-based models with mesh reconstruction (Yang et al. 2022; Darnon et al. 2022; Li et al. 2023; Oechsle, Peng, and Geiger 2021; Wang et al. 2021). For example, some works optimize neural signed distance functions (SDF) by training neural radiance fields (NeRF) in which the density is derived as a differentiable transformation of the SDF (Li et al. 2023; Oechsle, Peng, and Geiger 2021). A triangle mesh can finally be reconstructed from the SDF by applying the Marching Cubes algorithm (Lorensen and Cline 1987). Notably, SuGaR (Gu’edon and Lepetit 2023) introduced the pioneering method for high-precision scene mesh reconstruction from a 3DGS model. In contrast, our frameworks focus on specific target mesh reconstruction from scenes.

3D Reconstruction from Partial Views

Vanilla methods like NeRF (Mildenhall et al. 2020) or 3DGS (Ye et al. 2023) struggle in reconstruction under partial-view settings. Some research efforts focused on incorporating auxiliary priors, such as depth maps (Song et al. 2023; Wang et al. 2023), information theory (Kim, Seo, and Han 2022), symmetry (Seo, Chang, and Kwak 2023), and continuity (Niemeyer et al. 2022) to infer missing information. However, these approaches tend to be either too simplistic or overly specialized for certain scenes, resulting in poor generalization.

The recent progress in text-to-image diffusion models (Rombach et al. 2022) and their tailored applications (Poole et al. 2022; Wang et al. 2024) in the 3D field make it possible for reasonable novel-view synthesis, paving the way for impactful applications such as single-view 3D asserts generation (image-to-3d) (Liu et al. 2023a, 2024; Tang et al. 2023) and sparse reconstruction (Wynn and Turmukhambetov 2023; Xie et al. 2023; Liu et al. 2023b; Wu et al. 2024; Yang et al. 2024). However, existing sparse reconstruction methods are designed for scenarios where camera views are sparsely distributed across a 360 range. In contrast, our approach aims to reconstruct partially occluded targets by focusing on cases where views are densely clustered within the visible range of the target, while the occluded views remain entirely absent.

Method

Our framework aims to reconstruct the precise mesh of the target object from multi-view scene images. It comprises two main components: Target Gaussian Segmentation

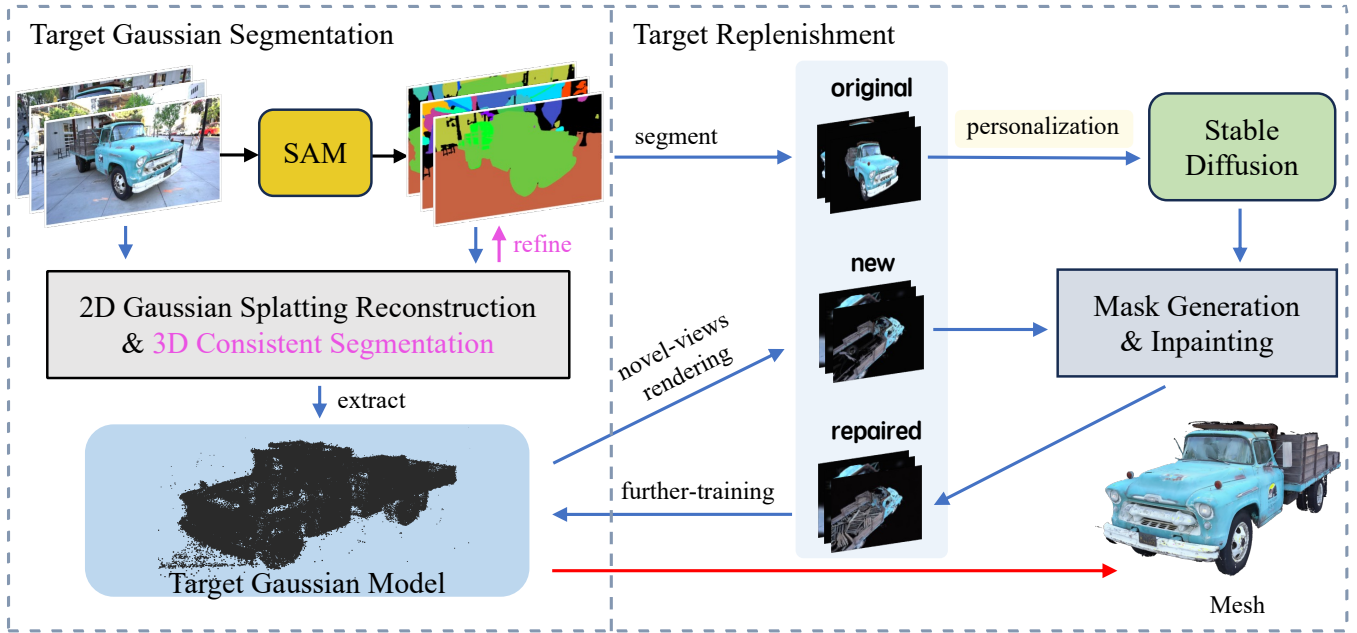


Figure 2: The framework of **OMEGAS**. OMEGAS comprises two stages: **Target Gaussian Segmentation** to segment target 2DGS model from multi-view images and provide accurate 3D consistent masks; **Target Replenishment** to optimize the target model by personalized Stable Diffusion with a Mask-generation & Inpainting process. The final object mesh is extracted from the optimized target Gaussian model.

(TGS) to segment the 3D target from multi-view scene images and Target Replenishment (TR) to optimize the target by large-scale diffusion priors, as illustrated in Figure 2.

The rest of this section is organized as follows: in section *Preliminaries*, we introduce some basic concepts involved in this section, including 2D Gaussian Splatting (Huang et al. 2024) and the generative priors. In section *Target Gaussian Segmentation*, we introduce the technique that segments the initial 3D target from multi-view images by 2D Gaussian Splatting. In section *Target Replenishment*, we introduce the process that adaptively optimizes the target model by diffusion priors.

Preliminaries

2D Gaussian Splatting (2DGS) (Huang et al. 2024). Due to the multi-view inconsistent nature of 3D Gaussians, 3D Gaussian Splatting (3DGS) fails to accurately represent surfaces. Thus, Huang et al. proposed 2D Gaussian Splatting, which collapses the 3D volume into a set of 2D oriented planar Gaussian disks and provides view-consistent geometry while modeling surfaces intrinsically. Specifically, a 2D Gaussian is defined in a local tangent plane in world space, which is parameterized:

$$P(u, v) = \mathbf{p}_k + s_u \mathbf{t}_u u + s_v \mathbf{t}_v v = \mathbf{H}(u, v, 1, 1)^\top \quad (1)$$

$$\text{where } \mathbf{H} = \begin{bmatrix} s_u \mathbf{t}_u & s_v \mathbf{t}_v & 0 & \mathbf{p}_k \\ 0 & 0 & 0 & 1 \end{bmatrix} = \begin{bmatrix} \mathbf{RS} & \mathbf{p}_k \\ 0 & 1 \end{bmatrix} \quad (2)$$

where a 2D Gaussian plane $P(u, v)$ is defined by its central point \mathbf{p}_k , principal tangential vectors \mathbf{t}_u and \mathbf{t}_v , scaling vectors s_u and s_v . $\mathbf{H} \in 4 \times 4$ is the homogeneous transforma-

tion matrix representing the geometry of the 2D Gaussian. For the point $\mathbf{u} = (u, v)$ in uv space, its 2D Gaussian value is evaluated by standard Gaussian:

$$\mathbf{G}(\mathbf{u}) = \exp\left(-\frac{u^2 + v^2}{2}\right) \quad (3)$$

The center \mathbf{p}_k , scaling (s_u, s_v) , and the rotation $(\mathbf{t}_u, \mathbf{t}_v)$ are learnable parameters. Our framework harnesses the 2DGS model as the target reconstruction carrier due to its meticulous object reconstruction capabilities.

Text-to-Image Generative Priors & Personalization. In the past few years, with the advent of diffusion-based generative techniques, the community has developed numerous mature open-world large-scale generative models, *e.g.*, Stable Diffusion (Rombach et al. 2022). Technically, given input image $x \in \mathbf{R}^{H \times W \times 3}$, an encoder of variational auto-encoder (VAE) \mathcal{E} converts it into a latent representation $z_0 \in \mathbf{R}^{h \times w \times c}$, where image is downsampled by a factor f and channels are increased to c . Then a text-conditioned UNet ϵ_θ in latent space is used to predict the noise of each timestamp t from z_t and prompt y to recover z_0 , where θ is the param of UNet. After the denoising process, VAE’s decoder \mathcal{D} transforms z_0 to image space to generate the image.

The personalization of diffusion priors (Ruiz et al. 2023; Cao et al. 2024) is a technique that concentrates prior knowledge on a specific object by transforming or fine-tuning UNet parameters θ into a form specific to the given few object images, represented as ϵ_{θ^*} .

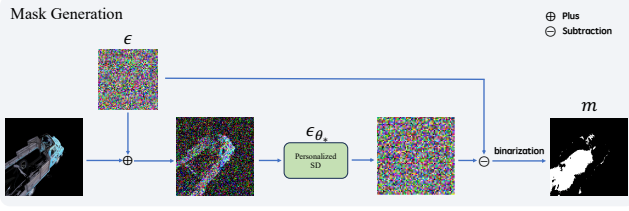


Figure 3: Mask generation process.

Target Gaussian Segmentation (TGS)

As depicted in the left part of Figure 2, we begin by introducing a novel technique known as Target Gaussian Segmentation. This method segments 3D-consistent target masks from multi-view images and extracts a preliminary 2DGS model of the target. The process is as follows.

Scene Segmentation by SAM. We first conduct preliminary target consistency segmentation on scene images from different views based on SAM’s capabilities in open-world segmentation for intricate scenes. Specifically, following the approach in (Ye et al. 2023), we treat the scene images from divergent views as a continuous video sequence and input them into SAM for initial segmentation. Next, by applying a zero-shot tracker (Cheng et al. 2023) to these segmentation results, we obtain unique object IDs ranging from 0 to 255. The segmented outcomes are preserved as gray-scale images, with each object’s ID represented in corresponding gray-scale values.

Target 2DGS Reconstruction & 3D Consistent Segmentation. We leverage the gray-scale images to guide the segmentation of 2DGS. We treat the gray scale as attributes similar to RGB colors for training 2D Gaussians. Similar to representing Gaussian colors using spherical harmonics coefficients, we add identity vectors to 2D Gaussians following (Mirzaei et al. 2023; Ye et al. 2023). To reduce the memory usage and training time, we set the identity vectors as length 8, encoding segmentation labels ranging from 0 to 255. When a 2D Gaussian is observed from a slanted views, the object-space low-pass filter is utilized:

$$\hat{\mathbf{G}}(\mathbf{x}) = \max \left\{ \mathbf{G}(\mathbf{u}(\mathbf{x})), \mathbf{G}\left(\frac{\mathbf{x} - \mathbf{c}}{\sigma}\right) \right\} \quad (4)$$

where \mathbf{c} is the projection of center \mathbf{p}_k .

By conducting differentiable rendering of identity vectors, similar to rendering colors, by blending \mathcal{N} ordered Gaussians on overlapping pixels, we can calculate the identity vectors O of pixels:

$$O(\mathbf{x}) = \sum_{i \in \mathcal{N}} o_i \alpha'_i \hat{\mathbf{G}}_i(\mathbf{u}(\mathbf{x})) \prod_{j=1}^{i-1} (1 - \alpha'_j \hat{\mathbf{G}}_j(\mathbf{u}(\mathbf{x}))) \quad (5)$$

where o_i represents the identity vector of each Gaussian, and α'_i is given by evaluating the opacity of 2D Gaussians multiplied by the opacity of each point. Unlike colors, the identity vectors of the same object does not change with different viewpoints, so we set the SH degree to 0, reducing computational complexity.

Segment Loss. Next, we use the 3D consistency of 2DGS to optimize the consistency of segmentation results on the scene images. The L1 loss and SSIM loss in the original 2DGS would lead to the inability to fit object labels. To address this issue, we introduce classification loss and 3D cosine similarity loss. Specifically: 1) for classification loss, we input the rendered identity vectors O into a linear layer f followed by a softmax operation:

$$F(O) = \text{softmax}(f(O)) \quad (6)$$

Then we use the standard cross-entropy loss L_{oe} for classification; 2) For the 3D cosine similarity loss, we sample m 2D Gaussians, ensuring that the cosine similarity of the identity features F_o from the n nearest 2D Gaussians is closely aligned:

$$L_{cs} = \frac{1}{mn} \sum_{j=1}^m \sum_{i=1}^n \frac{F(o_j) \cdot F(o_i)}{\|F(o_j)\| \|F(o_i)\|}$$

Making similar identity vectors closer can improve the 3D consistency of segmentation, thus enhancing segmentation accuracy. The total loss function is the weighted sum of the segmentation loss function and the original 2D Gaussian loss function L_{gs} :

$$L = L_{gs} + \lambda_{oe} L_{oe} + \lambda_{cs} L_{cs} \quad (7)$$

3D Consistent Segmentation. After training the 2DGS model to convergence, we extract the target model using its object ID. By rendering this model back into the original views, we obtain precise and 3D-consistent target masks.

Target Replenishment (TR)

As shown in the right section of Figure 2, after segmenting the target objects, we extract the target 2DGS model and obtain precise target masks in the view images. We then utilize generative diffusion priors to adaptively replenish the unseen portions and further refine the target model. In summary, we render the unseen view of the target Gaussian model, inpaint the areas that are not sufficiently reconstructed by Stable Diffusion, and then feed the inpainted images for further training.

Stable Diffusion Personalization. To focus the knowledge of large-scale diffusion priors on a specific target, we employ a personalization method to control Stable Diffusion. Specifically, we input the target images \tilde{I} , segmented from the original views, into a personalization model \mathcal{P} (e.g., DreamBooth (Ruiz et al. 2023)).

$$\epsilon_{\theta^*} = \mathcal{P}(\tilde{I}, \epsilon_{\theta}) \quad (8)$$

where ϵ_{θ} is the UNet of original Stable Diffusion with parameter θ , and ϵ_{θ^*} is the UNet of personalized SD.

Mask Generation & Inpainting. We then use the personalized SD to generate the poorly reconstructed mask of the novel-view rendering of the target Gaussian model, as depicted in Figure 3. Specifically, given a novel-view image x_0 , we encode it into latent space by the VAE encoder \mathcal{E} .

$$z_0 = \mathcal{E}(x_0) \quad (9)$$



Figure 4: Results of meshes with OMEGAS on the Instruct-NerF2NerF dataset(line 1), Tanks&Temples dataset(line 2), LERF dataset(line 3,4,5) and Mip-Nerf360 dataset(line 6).

We then perturb z_0 by diffusion forward process with noise ϵ :

$$z_t = \sqrt{\alpha_t} z_0 + \sqrt{1 - \alpha_t} \epsilon, \quad \epsilon \sim \mathcal{N}(0, \mathbf{I}),$$

where $\mathcal{N}(0, \mathbf{I})$ is a Gaussian Distribution, t denotes the timestep sampled from $[0, T]$, z_t represents perturbed z_0 at t , and α_t is predefined noise scheduling coefficient.

By applying the personalized UNet ϵ_{θ^*} , we can get the noise residual by:

$$\Delta \epsilon = \epsilon_{\theta^*}(z_t, y, t) - \epsilon,$$

where $\Delta \epsilon$ is the latent noise residual, y represents the embedded text prompt, which we set to empty based on experimental results.

The final inpainting mask m is given by:

$$m = \mathcal{B} \circ \mathcal{D}(\Delta \epsilon),$$

where \mathcal{D} is the VAE decoder, and \mathcal{B} is the image binarization operator.

Subsequently, the mask m and the novel-view image x_0

are input into a standard Stable Diffusion inpainting model¹, resulting in the final fixed image \tilde{x}_0 .

Mesh Extraction. By generating n novel-view images $X = \{x_0^i\}_{i=0}^{n-1}$ and applying the inpainting process, we obtain n refined images $\tilde{X} = \{\tilde{x}_0^i\}_{i=0}^{n-1}$. These refined images are then fed into the target 2DGS model for further training, addressing deficiencies in the first stage.

Ultimately, following Huang et al., to obtain meshes from the reconstructed 2D splats, we generate depth maps of the training views by projecting the splats' depth values onto the pixels. We then apply truncated signed distance fusion (TSDF) using Open3D to merge the reconstructed depth maps.

Experiments

Implementation Details

All experiments are performed and measured on a single GPU NVIDIA RTX 3090 with Ubuntu 18.04 LTS.

¹huggingface.co/stabilityai/stable-diffusion-2-inpainting

Table 1: Comparison of segmentation on LERF-MASK dataset (Ye et al. 2023). We adopt mIoU and boundary metrics mBIoU for better segmentation quality measurement. We also compared the average memory required for training. The empirical evidence substantiates that our methodology yields superior outcomes in both quality and efficiency.

Model	Memory GB ↓	mIoU↑	figurines mBIoU↑	time↓	mIoU↑	ramen mBIoU↑	time↓	mIoU↑	teatime mBIoU↑	time↓
SAM		74.83	73.71		57.25	56.99		75.95	74.48	
Gaussian Grouping (7k iter)	21	86.08	84.08	7min	70.34	58.03	7min	75.98	71.91	7min
Ours (7k iter)	10	86.21	84.09	6min	86.48	73.62	5min	78.81	73.32	6min
Ours (30k iter)	13	88.86	86.65	65min	88.63	75.93	51min	79.41	73.37	64min



Figure 5: Comparing mesh extracting results with SuGaR, 2D Gaussian Splatting and DreamGaussian. The scenes are selected from LERF and Instruct-NerF2NeRF datasets. Both SuGaR, 2DGS, and our approach use multi-view images as input, while DreamGaussian relies on a single-view image.

Datasets. To evaluate the reconstruction quality, we tested our OMEGAS on scenes presented in LERF-MASK dataset (Ye et al. 2023) and Mip-Nerf360 dataset (Barron et al. 2022), where the flowers and treehill are skipped due to the non-public access right. We also take diverse 3D scene cases from LERF (Kerr et al. 2023), Tanks&Temples (Knapitsch et al. 2017) and Instruct-NerF2NeRF (Haque et al. 2023) for visual comparison.

Model Details. In Target Gaussian Segmentation, we take SAM-HQ model (Ke et al. 2023) for initial segmentation. The confidence threshold p_{ex} for extraction is 0.95. We use the Adam (Kingma and Ba 2014) optimizer for both Gaussians and linear and train for max 30000 iterations with a learning rate of 0.0025 for identity vectors and 0.0005 for linear layer. For 3D regularization loss, we choose $n = 5$ and $m = 1000$. We employ Principal Component Analysis

Table 2: Quantitative results of target mesh extraction on the Tanks & Temples dataset (Knapitsch et al. 2017), represented by F1 score.

Model	Truck	Ignatius	Caterpillar	Mean
SuGaR	0.0741	0.1392	0.1827	0.1320
Dream Gaussian	0.0013	0.0007	0.0031	0.0017
2DGS	0.1421	0.3423	0.2100	0.2315
Ours	0.1635	0.4464	0.2208	0.2769

as a means to visualize the outcomes of the segmentation.

In Target Replenishment, we adopt Stable Diffusion 2.1 with the resolution 512x512. We take DreamBooth (Ruiz et al. 2023) as our personalization model. When generating a mask, we fix the timestep t to 991 and sample 10 random seeds to obtain an averaged mask result.

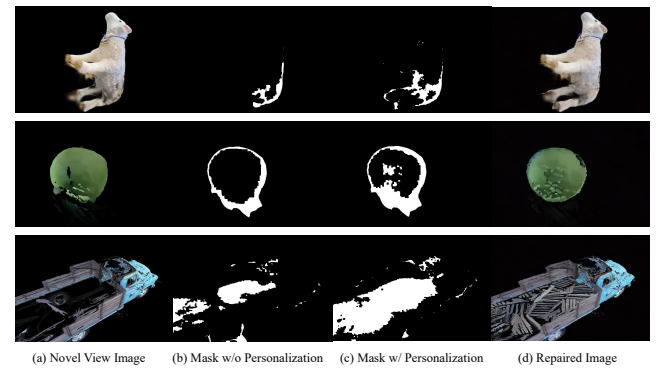


Figure 6: Effect of personalization and inpainting. It shows the mask w/ or w/o personalization of SD and the inpainting results on the Tanks&Temples dataset and LERF dataset.

Comparative Analysis

Target Mesh Extraction. To demonstrate the effectiveness of our target mesh extraction method, we provide qualitative comparisons with the scene reconstruction approach SuGaR (Gu’edon and Lepetit 2023) and 2DGS (Huang et al. 2024). Since our method is the first to tackle target reconstruction in a multi-view context, we are limited to using the single-view method DreamGaussian (Tang et al. 2023) as our other target reconstruction comparative baseline. The



Figure 7: Effect of the Target Replenishment (TR) Module. The first line shows the mesh generated solely using Target Gaussian Segmentation. The second line displays the mesh produced by our complete model, including the Target Replenishment module.

results are presented in Figure 5, showcasing detailed qualitative outcomes across various open-world scenarios, including teatime, bear, and kitchen from the LERF (Kerr et al. 2023) and Instruct-NeRF2NeRF (Haque et al. 2023) datasets. Both SuGaR, 2DGS, and our approach use multi-view images as input, while DreamGaussian relies on a single-view image.

Compared to SuGaR and 2DGS, our method achieves superior detail across all three scenes. SuGaR and 2DGS’s focus on the overall scene lead to a noticeable reduction in the granularity of local details. In the bear scene, our method demonstrates its capability to reconstruct unseen portions in the input view. Meanwhile, the kitchen scene highlights the precision of our approach in segmenting and extracting complex objects. Compared to DreamGaussian, our method significantly enhances the quality of the generated meshes.

We also conduct quantitative experiments in Table 2 on the Tanks & Temples dataset (Knapitsch et al. 2017). Since our method focuses on mesh extraction of target objects within a scene, we manually removed other objects from the ground truth mesh to quantify the accuracy of our approach. For methods that cannot isolate the target object, we used the complete ground truth mesh to ensure fairness. We employed the evaluation metrics provided by the Tanks&Temples dataset (Knapitsch et al. 2017), calculating precision and recall to obtain the F1 score. Our method consistently achieves superior results across all scenarios in the dataset compared to other methods.

In Figure 4, we further demonstrate the mesh quality and highlight our method’s effectiveness in extracting small objects from complex scenes.

Scene Segmentation. To demonstrate the effectiveness of our Gaussian Segmentation method, we conducted quantitative scene segmentation experiments on the LERF-MASK dataset (Kerr et al. 2023), using Gaussian Grouping (Ye et al. 2023), as shown in Table 1. Due to VRAM limitations, we trained Gaussian Grouping for a max of 7,000 iterations on

a single NVIDIA RTX 3090 GPU. Despite these constraints, our method achieved considerable improvements under the same iteration settings, with lower memory usage and reduced training time across three scenes. When further training our method for 30,000 iterations, we observed more performance gains.

Ablations

In this section, we isolate the design choices and evaluate their impacts, including the effect of the Target Replenishment stage and the necessity of personalizing SD.

Effect of Target Replenishment (TR). We first examine the effects of the proposed Target Replenishment module, as shown in Figure 7. It shows the difference between mesh results w/ and w/o TR module on an example of Tanks&Temples dataset (Knapitsch et al. 2017). Specifically, there are no images taken from above or showing the interior of the truck’s carriage in the given dataset views. Without TR, a significant mesh hole would appear inside the truck, whereas our method can properly fill the mesh.

Effect of Personalizing SD. We now analyze the effect of personalizing SD to generate inpainting masks in Figure 6. In the figure, (a) are images of the object rendered from a random viewpoint, (b) are masks generated by a standard Stable Diffusion model, (c) are masks generated by a personalized Stable Diffusion model, and (d) are inpainted images by mask (c). It can be observed that the mask generated by the personalized Stable Diffusion model covers a larger area and more accurately identifies the locations of the holes, resulting in a better-repaired image.

Conclusion

We present OMEGAS: Object Mesh Extraction from Large Scenes Guided by Gaussian Segmentation. OMEGAS efficiently extracts high-precision meshes of target objects from multi-view scene images and can reconstruct occluded or invisible parts of the targets. OMEGAS introduces a novel

Target Gaussian Segmentation technique, which segments the target Gaussian model from multi-view images using 2D Gaussian Splatting. Additionally, OMEGAS proposes a Target Replenishment technique that leverages open-world diffusion priors to address unseen portions of the target.

References

- Barron, J. T.; Mildenhall, B.; Verbin, D.; Srinivasan, P. P.; and Hedman, P. 2022. Mip-nerf 360: Unbounded anti-aliased neural radiance fields. In *Proceedings of the IEEE/CVF Conference on Computer Vision and Pattern Recognition*, 5470–5479.
- Caetano, I.; Santos, L.; and Leitão, A. 2020. Computational design in architecture: Defining parametric, generative, and algorithmic design. *Frontiers of Architectural Research*, 9(2): 287–300.
- Cao, P.; Zhou, F.; Song, Q.; and Yang, L. 2024. Controllable generation with text-to-image diffusion models: A survey. *arXiv preprint arXiv:2403.04279*.
- Cheng, H. K.; Oh, S. W.; Price, B.; Schwing, A.; and Lee, J.-Y. 2023. Tracking anything with decoupled video segmentation. In *Proceedings of the IEEE/CVF International Conference on Computer Vision*, 1316–1326.
- Darmon, F.; Bascle, B.; Devaux, J.-C.; Monasse, P.; and Aubry, M. 2022. Improving neural implicit surfaces geometry with patch warping. In *Proceedings of the IEEE/CVF Conference on Computer Vision and Pattern Recognition*, 6260–6269.
- Fan, S.; Dong, Q.; Zhu, F.; Lv, Y.; Ye, P.; and Wang, F.-Y. 2021. SCF-Net: Learning spatial contextual features for large-scale point cloud segmentation. In *Proceedings of the IEEE/CVF Conference on Computer Vision and Pattern Recognition*, 14504–14513.
- Goessele, M.; Snavely, N.; Curless, B.; Hoppe, H.; and Seitz, S. M. 2007. Multi-view stereo for community photo collections. In *2007 IEEE 11th International Conference on Computer Vision*, 1–8. IEEE.
- Gu’edon, A.; and Lepetit, V. 2023. SuGaR: Surface-Aligned Gaussian Splatting for Efficient 3D Mesh Reconstruction and High-Quality Mesh Rendering. *ArXiv*, abs/2311.12775.
- Haque, A.; Tancik, M.; Efros, A.; Holynski, A.; and Kanazawa, A. 2023. Instruct-NeRF2NeRF: Editing 3D Scenes with Instructions. In *ICCV*.
- Huang, B.; Yu, Z.; Chen, A.; Geiger, A.; and Gao, S. 2024. 2d gaussian splatting for geometrically accurate radiance fields. In *ACM SIGGRAPH 2024 Conference Papers*, 1–11.
- Ke, L.; Ye, M.; Danelljan, M.; Liu, Y.; Tai, Y.-W.; Tang, C.-K.; and Yu, F. 2023. Segment Anything in High Quality. In *NeurIPS*.
- Kerbl, B.; Kopanas, G.; Leimkühler, T.; and Drettakis, G. 2023. 3d gaussian splatting for real-time radiance field rendering. *ACM Transactions on Graphics*, 42(4): 1–14.
- Kerr, J.; Kim, C. M.; Goldberg, K.; Kanazawa, A.; and Tancik, M. 2023. LERF: Language Embedded Radiance Fields. In *ICCV*.
- Kim, M.; Seo, S.; and Han, B. 2022. Infonerf: Ray entropy minimization for few-shot neural volume rendering. In *Proceedings of the IEEE/CVF Conference on Computer Vision and Pattern Recognition*, 12912–12921.
- Kingma, D. P.; and Ba, J. 2014. Adam: A Method for Stochastic Optimization. *CoRR*, abs/1412.6980.
- Kirillov, A.; Mintun, E.; Ravi, N.; Mao, H.; Rolland, C.; Gustafson, L.; Xiao, T.; Whitehead, S.; Berg, A. C.; Lo, W.-Y.; et al. 2023. Segment anything. In *ICCV*.
- Knapitsch, A.; Park, J.; Zhou, Q.-Y.; and Koltun, V. 2017. Tanks and temples: Benchmarking large-scale scene reconstruction. *ACM Transactions on Graphics (ToG)*, 36(4): 1–13.
- Li, Z.; Müller, T.; Evans, A.; Taylor, R. H.; Unberath, M.; Liu, M.-Y.; and Lin, C.-H. 2023. Neuralangelo: High-fidelity neural surface reconstruction. In *Proceedings of the IEEE/CVF Conference on Computer Vision and Pattern Recognition*, 8456–8465.
- Liu, M.; Xu, C.; Jin, H.; Chen, L.; Varma, T. M.; Xu, Z.; and Su, H. 2024. One-2-3-45: Any single image to 3d mesh in 45 seconds without per-shape optimization. *Advances in Neural Information Processing Systems*, 36.
- Liu, R.; Wu, R.; Hoorick, B. V.; Tokmakov, P.; Zakharov, S.; and Vondrick, C. 2023a. Zero-1-to-3: Zero-shot One Image to 3D Object. *2023 IEEE/CVF International Conference on Computer Vision (ICCV)*, 9264–9275.
- Liu, X.; Chen, J.; Kao, S.-h.; Tai, Y.-W.; and Tang, C.-K. 2023b. Deceptive-nerf: Enhancing nerf reconstruction using pseudo-observations from diffusion models. *arXiv preprint arXiv:2305.15171*.
- Lorensen, W. E.; and Cline, H. E. 1987. Marching cubes: A high resolution 3D surface construction algorithm. *Proceedings of the 14th annual conference on Computer graphics and interactive techniques*.
- Mildenhall, B.; Srinivasan, P. P.; Tancik, M.; Barron, J. T.; Ramamoorthi, R.; and Ng, R. 2020. NeRF: Representing Scenes as Neural Radiance Fields for View Synthesis. In *ECCV*.
- Mirzaei, A.; Aumentado-Armstrong, T.; Derpanis, K. G.; Kelly, J.; Brubaker, M. A.; Gilitschenski, I.; and Levinshtein, A. 2023. SPIn-NeRF: Multiview segmentation and perceptual inpainting with neural radiance fields. In *CVPR*.
- Niemeyer, M.; Barron, J. T.; Mildenhall, B.; Sajjadi, M. S.; Geiger, A.; and Radwan, N. 2022. Regnerf: Regularizing neural radiance fields for view synthesis from sparse inputs. In *Proceedings of the IEEE/CVF Conference on Computer Vision and Pattern Recognition*, 5480–5490.
- Oechsle, M.; Peng, S.; and Geiger, A. 2021. Unisurf: Unifying neural implicit surfaces and radiance fields for multi-view reconstruction. In *Proceedings of the IEEE/CVF International Conference on Computer Vision*, 5589–5599.
- Poole, B.; Jain, A.; Barron, J. T.; and Mildenhall, B. 2022. Dreamfusion: Text-to-3d using 2d diffusion. *arXiv preprint arXiv:2209.14988*.
- Rombach, R.; Blattmann, A.; Lorenz, D.; Esser, P.; and Ommer, B. 2022. High-resolution image synthesis with latent

- diffusion models. In *Proceedings of the IEEE/CVF conference on computer vision and pattern recognition*, 10684–10695.
- Ruiz, N.; Li, Y.; Jampani, V.; Pritch, Y.; Rubinstein, M.; and Aberman, K. 2023. Dreambooth: Fine tuning text-to-image diffusion models for subject-driven generation. In *Proceedings of the IEEE/CVF conference on computer vision and pattern recognition*, 22500–22510.
- Seo, S.; Chang, Y.; and Kwak, N. 2023. Flipnerf: Flipped reflection rays for few-shot novel view synthesis. In *Proceedings of the IEEE/CVF International Conference on Computer Vision*, 22883–22893.
- Siciliano, B.; Khatib, O.; and Kröger, T. 2008. *Springer handbook of robotics*, volume 200. Springer.
- Snavely, N.; Seitz, S. M.; and Szeliski, R. 2006. Photo tourism: exploring photo collections in 3D. In *ACM siggraph 2006 papers*, 835–846. Association for Computing Machinery.
- Song, J.; Park, S.; An, H.; Cho, S.; Kwak, M.-S.; Cho, S.; and Kim, S. 2023. D²RF: boosting radiance fields from sparse inputs with monocular depth adaptation. In *Proceedings of the 37th International Conference on Neural Information Processing Systems*, 68458–68470.
- Tang, J.; Ren, J.; Zhou, H.; Liu, Z.; and Zeng, G. 2023. Dreamgaussian: Generative gaussian splatting for efficient 3d content creation. *arXiv preprint arXiv:2309.16653*.
- Wang, G.; Chen, Z.; Loy, C. C.; and Liu, Z. 2023. Sparsenerf: Distilling depth ranking for few-shot novel view synthesis. In *Proceedings of the IEEE/CVF International Conference on Computer Vision*, 9065–9076.
- Wang, P.; Liu, L.; Liu, Y.; Theobalt, C.; Komura, T.; and Wang, W. 2021. Neus: Learning neural implicit surfaces by volume rendering for multi-view reconstruction. *arXiv preprint arXiv:2106.10689*.
- Wang, Z.; Lu, C.; Wang, Y.; Bao, F.; Li, C.; Su, H.; and Zhu, J. 2024. Prolificdreamer: High-fidelity and diverse text-to-3d generation with variational score distillation. *Advances in Neural Information Processing Systems*, 36.
- Wu, G.; Yi, T.; Fang, J.; Xie, L.; Zhang, X.; Wei, W.; Liu, W.; Tian, Q.; and Wang, X. 2023. 4d gaussian splatting for real-time dynamic scene rendering. *arXiv preprint arXiv:2310.08528*.
- Wu, R.; Mildenhall, B.; Henzler, P.; Park, K.; Gao, R.; Watson, D.; Srinivasan, P. P.; Verbin, D.; Barron, J. T.; Poole, B.; et al. 2024. Reconfusion: 3d reconstruction with diffusion priors. In *Proceedings of the IEEE/CVF Conference on Computer Vision and Pattern Recognition*, 21551–21561.
- Wynn, J.; and Turmukhambetov, D. 2023. Diffusionerf: Regularizing neural radiance fields with denoising diffusion models. In *Proceedings of the IEEE/CVF Conference on Computer Vision and Pattern Recognition*, 4180–4189.
- Xie, Y.; Xu, C.; Rakotosaona, M.-J.; Rim, P.; Tombari, F.; Keutzer, K.; Tomizuka, M.; and Zhan, W. 2023. Sparsefusion: Fusing multi-modal sparse representations for multi-sensor 3d object detection. In *Proceedings of the IEEE/CVF International Conference on Computer Vision*, 17591–17602.
- Xiong, J.; Hsiang, E.-L.; He, Z.; Zhan, T.; and Wu, S.-T. 2021. Augmented reality and virtual reality displays: emerging technologies and future perspectives. *Light: Science & Applications*, 10(1): 1–30.
- Xu, C.; Wu, B.; Wang, Z.; Zhan, W.; Vajda, P.; Keutzer, K.; and Tomizuka, M. 2020. Squeezesegv3: Spatially-adaptive convolution for efficient point-cloud segmentation. In *Computer Vision–ECCV 2020: 16th European Conference, Glasgow, UK, August 23–28, 2020, Proceedings, Part XXVIII 16*, 1–19. Springer.
- Yang, B.; Bao, C.; Zeng, J.; Bao, H.; Zhang, Y.; Cui, Z.; and Zhang, G. 2022. Neumesh: Learning disentangled neural mesh-based implicit field for geometry and texture editing. In *European Conference on Computer Vision*, 597–614. Springer.
- Yang, C.; Li, S.; Fang, J.; Liang, R.; Xie, L.; Zhang, X.; Shen, W.; and Tian, Q. 2024. Gaussianobject: Just taking four images to get a high-quality 3d object with gaussian splatting. *arXiv preprint arXiv:2402.10259*.
- Yang, Z.; Gao, X.; Zhou, W.; Jiao, S.; Zhang, Y.; and Jin, X. 2023. Deformable 3d gaussians for high-fidelity monocular dynamic scene reconstruction. *arXiv preprint arXiv:2309.13101*.
- Ye, M.; Danelljan, M.; Yu, F.; and Ke, L. 2023. Gaussian Grouping: Segment and Edit Anything in 3D Scenes. *ArXiv*, abs/2312.00732.
- Yu, A.; Ye, V.; Tancik, M.; and Kanazawa, A. 2021. pixelnerf: Neural radiance fields from one or few images. In *Proceedings of the IEEE/CVF Conference on Computer Vision and Pattern Recognition*, 4578–4587.